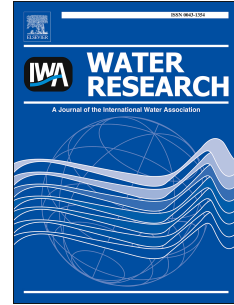# Journal Pre-proof

A knowledge discovery framework to predict the N_2O emissions in the wastewater sector

V. Vasilaki, V. Conca, N. Frison, A.L. Eusebi, F. Fatone, E. Katsou

Please cite this article as: Vasilaki, V., Conca, V., Frison, N., Eusebi, A.L., Fatone, F., Katsou, E., A knowledge discovery framework to predict the N_2O emissions in the wastewater sector, *Water Research* (2020), doi: https://doi.org/10.1016/j.watres.2020.115799.

This is a PDF file of an article that has undergone enhancements after acceptance, such as the addition of a cover page and metadata, and formatting for readability, but it is not yet the definitive version of record. This version will undergo additional copyediting, typesetting and review before it is published in its final form, but we are providing this version to give early visibility of the article. Please note that, during the production process, errors may be discovered which could affect the content, and all legal disclaimers that apply to the journal pertain.
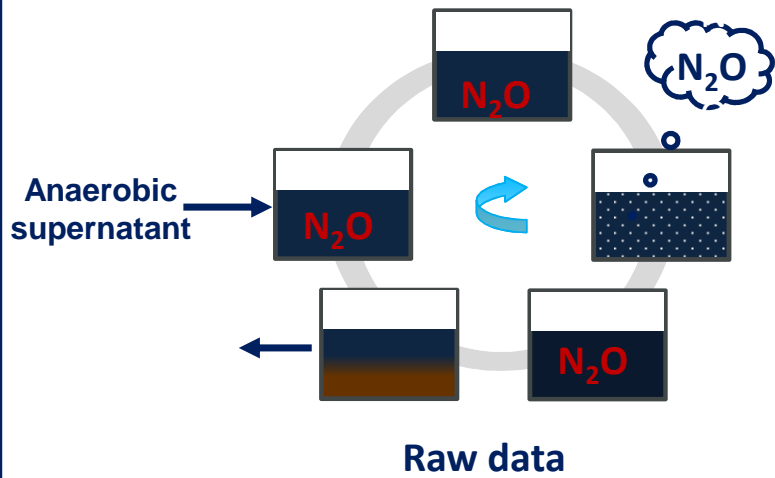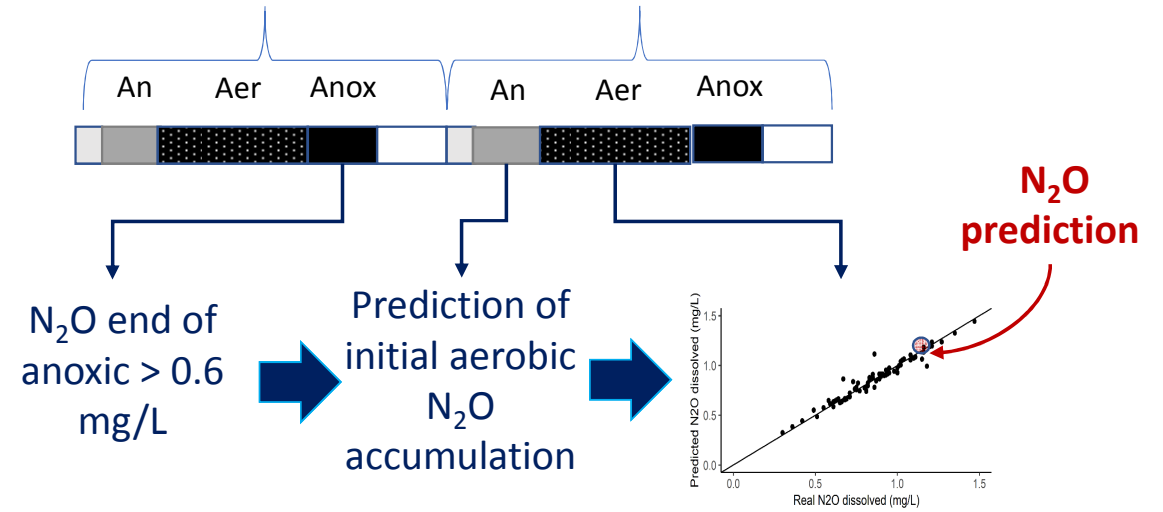
1   **A knowledge discovery framework to predict the** N_2O **emissions in the wastewater sector**

2   V. Vasilaki[1], V. Conca[2], N. Frison[2], A.L. Eusebi[3], F. Fatone[3], E. Katsou[1*]

3   [1] Department of Civil & Environmental Engineering, Brunel University London, Uxbridge UB8
4   3PH, UK,

5   [2] Department of Biotechnology, University of Verona, Strada Le Grazie 15, 37134 Verona, Italy,

6   [3] Department SIMAU, Faculty of Engineering, Polytechnic University of Marche, Via Brecce
7   Bianche 12, Ancona, Italy

8   *Corresponding author. Email: evina.katsou@brunel.ac.uk

11   **Abstract**

12   Data Analytics is being deployed to predict the dissolved nitrous oxide (N_2O) concentration in a

13   full-scale sidestream sequence batch reactor (SBR) treating the anaerobic supernatant. On

14   average, the N_2O emissions are equal to 7.6% of the NH_4-N load and can contribute up to 97 % to

15   the operational carbon footprint of the studied nitritation-denitritation and via-nitrite enhanced

16   biological phosphorus removal process (S.C.E.N.A). The analysis showed that average aerobic

17   dissolved N_2O concentration could significantly vary under similar influent loads, dissolved

18   oxygen (DO), pH and removal efficiencies. A combination of density-based clustering, support

19   vector machine (SVM), and support vector regression (SVR) models were deployed to estimate

20   the dissolved N_2O concentration and behaviour in the different phases of the SBR system.

21   The results of the study reveal that the aerobic dissolved N_2O concentration is correlated with the

22   drop of average aerobic conductivity rate (spearman correlation coefficient equal to 0.7), the DO

23   (spearman correlation coefficient equal to -0.7) and the changes of conductivity between

24   sequential cycles. Additionally, operational conditions resulting in low aerobic N_2O accumulation

25   (<0.6 mg/L) were identified; step-feeding, control of initial NH_4^+ concentrations and aeration

26   duration can mitigate the N_2O peaks observed in the system. The N_2O emissions during aeration

27   shows correlation with the stripping of accumulated N_2O from the previous anoxic cycle. The

28   analysis shows that N_2O is always consumed after the depletion of NO_2^- during denitritation (after

29   the "nitrite knee"). Based on these findings SVM classifiers were constructed to predict whether

30   dissolved N_2O will be consumed during the anoxic and anaerobic phases and SVR models were

31   trained to predict the N_2O concentration at the end of the anaerobic phase and the average

32   dissolved N_2O concentration during aeration. The proposed approach accurately predicts the N_2O

33   emissions as a latent parameter from other low-cost sensors that are traditionally deployed in

34   biological batch processes.

1. Introduction

In recent years the sustainability and operational efficiency of wastewater treatment plants (WWTPs) have come to the fore (Liu et al., 2018). Several biological technologies such as partial-nitritation – anammox (anaerobic ammonium oxidation) have emerged, towards the efficient, low-cost treatment of high-strength municipal wastewater streams (Lackner et al., 2014; Zhou et al., 2018). The anaerobic supernatant is a by-product of dewatering of the anaerobic digestion effluent and represents less than 1-2% of the total influent flow in the WWTP. It contains 10–30% of the N load and 20–30% of the P load (Janus and van der Roest, 1997; van Loosdrecht and Salem, 2006). Sidestream treatment of the anaerobic supernatant can contribute to the reduction of energy consumption for N-removal, decrease of nitrogen loads in the secondary treatment, and the minimisation of risks related to exceeding effluent regulatory requirements of nitrogen concentrations in the water line of WWTPs (Eskicioglu et al., 2018). However, the performance and environmental evaluation of different sidestream technologies is still under investigation (Eskicioglu et al., 2018; Rodriguez-Garcia et al., 2014).

SCENA (Short-Cut Enhanced Nutrient Abatement) is a new sidestream process, that combines the conversion of NH_4^+ to NO_2^- under aerobic conditions (nitritation) with the subsequent reduction of NO_2^- to nitrogen gas and enhanced biological phosphorus uptake by polyphosphate-accumulating organisms (DPAOs) in a sequencing batch reactor (SBR) (Frison et al., 2015). External volatile fatty acids (VFAs), are produced via acidogenic fermentation of the primary and secondary sludge on-site and dosed into the SBR. In a recent study, Longo et al. (2016), quantified the environmental and cost benefits and impacts of the integration of the SCENA process in a full-scale WWTP. They reported major energy savings for aeration after the integration of sidestream SCENA process. The direct N_2O emissions were equal to 1.42% of the

3

58 influent N-load. Short-term monitoring campaigns were implemented, while the effect of

59 operational conditions on N_2O generation was not investigated.

60 N_2O is a potent cause of global warming, its global warming potential is 265 - 298 times more

61 than that of CO_2 (IPCC, 2013). The emission of N_2O in full-scale sidestream partial-

62 nitritation/partial-nitritation–anammox or nitrification-denitrification systems range from 0.17%

63 to 5.1% of the influent N-load (average equal to ∼2.1% of the N-load is emitted (Vasilaki et al.,

64 2019) . Schaubroeck et al. (2015) showed that N_2O emissions from a full-scale sidestream

65 DEMON process in Austria were significantly higher than the direct N_2O emissions from the

66 mainstream treatment in a full-scale WWTP. On average, 0.256 g N_2O were emitted compared to

67 0.005 g emitted in the secondary treatment per m^3 treated wastewater. The increased direct N_2O

68 emissions can be mainly attributed to low DO concentrations, higher ammonia oxidation rates

69 (AOR) and NO_2^- build-up (Desloover et al., 2011; Kampschreur et al., 2008); conditions that also

70 prevail in the SCENA process. The variability of EF reported in sidestream technologies can be

71 partially attributed to both complex relationships between emitted N_2O and operational conditions

72 and different configurations (i.e. SBR, continuous systems), loads (i.e. NH_4^+ concentrations),

73 feeding strategies and operational control (i.e. DO set-points). Additionally, different interactions

74 between operational variables trigger a different response of N_2O generation. For instance, in a

75 recent modelling study of a granular one-stage partial-nitrition-anammox reactor, Wan et al.

76 (2019) showed that higher temperatures resulted in increased N_2O emissions in the presence of

77 COD (chemical oxygen demand) and in decreased N_2O emissions in the absence of COD (due to

78 increased anammox activity and reduction of NO_2^- accumulation in higher temperature).

79 Additionally, the long-term temporal variations of direct N_2O emissions were not adequately

80 assessed in sidestream technologies; the majority of the monitoring campaigns in sidestream

81 reactors lasted less than 5 days (Vasilaki et al., 2019).

82   The digitalisation of water services and the data-driven knowledge discovery from wastewater

83   treatment plant may increase the resilience of water utilities under climate change and other

84   water-related challenges (Sarni et al., 2019). Recent studies have provided extensive overviews of

85   the use of data-driven techniques in the wastewater sector for different applications including the

86   development of soft-sensors, fault prediction and multi-objective optimisation of control of water

87   utilities (Corominas et al., 2018a; Haimi et al., 2013; Newhart et al., 2019). Data-mining and

88   extraction of the information hidden in the raw sensor signals can facilitate the identification of

89   patterns and hidden structures and reveal significant information on the behaviour of N_2O

90   emissions in continuous wastewater treatment processes (Vasilaki et al., 2018). The SBR in the

91   SCENA process is multiphase (i.e. anaerobic, aerobic, anoxic conditions) applying different

92   operational variables (unsynchronised data), non-linear and subject to different disturbances, such

93   as influent compositions and fermentation liquid characteristics. Moreover, SBR process data are

94   based on a 3d-structure that consists of the number of i) cycles, ii) variables and iii) sampling

95   points within each cycle. Therefore, the identification of process abnormalities and patterns can

96   be complicated. N_2O emissions could be affected by both within-cycle and between-cycle batch

97   dynamics.

98   In this study, sensor and laboratory analyses data from a full-scale SCENA SBR were analysed to

99   provide insights on the N_2O emissions behaviour and generation. A structured approach was

100   followed for knowledge discovery from the available dataset using a combination of abnormal

101   events detection, classification and regression techniques. The objectives of the study were to i)

102   investigate whether the sensors integrated in the system (i.e. conductivity, pH) can provide

103   actionable information on the dynamics of N_2O emissions, ii) detect hotspots for the

104   accumulation and emission of N_2O and iii) develop data-driven regression and classification

105 models to predict the dissolved N_2O behaviour and concentration for the different phases

106 (anaerobic, aerobic, anoxic) of the SBR.

107 **2.   Materials and Methods**

108 **2.1   Process description and data origin**

109 The Carbonera plant is designed to treat domestic wastewater of a population equivalent of

110 40,000 (dry weather flow equal to 10,000 m^3/d). After screening and degritting and primary

111 sedimentation, the effluent from the primary clarifier is sent to a Schreiber reactor (single basin –

112 working volume 4671 m^3). Schreiber reactor effluent is pumped to two secondary clarifiers (2260

113 m^3 each) and subsequently to the tertiary treatment unit for disinfection and filtration before final

114 discharge in the Melma River.

115 Waste activated sludge (WAS) generated by the biological treatment is recycled to the primary

116 sedimentation unit and mixed with primary sludge. The final concentration of the thickened

117 mixed sludge is around 5% total solids (TS). About 90% of the mixed thickened sludge is fed to

118 an anaerobic digestion unit (1800 m^3 working volume). Digestate is dewatered by a centrifuge

119 with the addition of polyelectrolyte; the solid fraction is mechanically composted and used as

120 agricultural fertilizer. The anaerobic supernatant is sent to the equalization tank (of 90 m^3) in the

121 SCENA system for the biological N and P removal.

122 The remaining portion of mixed sludge (10%) is fed to a sequencing batch fermentation reactor

123 (SBFR) with hydraulic retention time (HRT) equal to 5 days. The SBFR is operated under

124 mesophilic condition (37°C) for the alkaline fermentation of thickened sewage sludge and the on-

125 site production of carbon source enriched of VFAs (mainly acetic and propionic acids). Daily, 10

126 m^3 of fermentation sludge are extracted and replaced with fresh thickened sludge. The solid/liquid

127 separation of the fermented sewage sludge is carried out by a screw-press (SCAE), generating ~2-

128   4 m^3/h of fermentation liquid rich of VFAs (in total, ~ 10.5 m^3/d). The latter is collected in a

129   storage tank of 20 m^3 and automatically dosed during the anaerobic and anoxic phases of a short-

130   cut sequencing batch reactor (SBR) based on pH and conductivity sensors. The solid fermented

131   fraction (13-15% TS based) is mixed with the thickened mixed sludge and fed to the anaerobic

132   digestor.

133   The anaerobic supernatant is treated in an SBR with a maximal working volume of 70 m^3 (3-4

134   cycles daily). The SBR is fed with ~10-15 m^3 of anaerobic supernatant in each cycle that is

135   treated via nitrite enhanced phosphorus removal associated with nitritation-denitritation

136   (S.C.E.N.A process). The typical SBR (Figure 1) cycle consists of feeding (6-8 min), anaerobic

137   conditions (30 min), aerobic conditions (200-240 min), anoxic (~60-140 min), settling (30 min)

138   and discharge (8 min). The sensors integrated in the SBR include: pH, Dissolved Oxygen (DO),

139   conductivity, Oxidation Reduction Potential (ORP), mixed liquor suspended Solids (MLSS) and

140   temperature. Conductivity and pH are used to control the length of the aerobic and anoxic phases

141   and the carbon source dosage. Additionally, variable frequency driver is used to control the air

142   flow-rate of the blowers, maintaining the dissolved oxygen during aerobic phase in the range of

143   1.0 to 1.5 mg/L. The aeration system consists of volumetric blowers (nominal power 11 kW) and

144   n80 diffusers (INVENT), providing ~500 m^3/h of compressed air at 400 mbar of pressure. The

145   treated supernatant is recirculated back to the WWTP headworks.

146   A monitoring campaign was conducted in the sidestream line at Carbonera WWTP treatment

147   plant for approximately 4 months (January 2019 – April 2019). Dissolved N_2O concentrations

148   were measured using a polarographic Clark-type electrode (Unisense, Aarhus, Denmark). To

149   supplement the long-term monitoring campaign with Unisense probes, N_2O emissions in the

150   headspace of the SBR reactor, were also continuously monitored with MIR9000CLD analyser

151   (Environment Italia S.p.A.) during March – April 2019. Details of the monitoring campaign, N_2O

152   emissions' calculation and laboratory analyses are provided in the supplementary material (S1-

153   S3).

154   [Figure 1]

155   **2.2   Data analysis**

156   2.2.1   *Methodological Framework*

157   Figure 2 summarises the methodological framework of the study. Phase one includes preliminary

158   analysis of the collected data. Features extraction and density-based clustering was applied (Ester

159   et al., 1996), to isolate abnormal cycles. The methodology and results of abnormal cycles'

160   isolation are given in the supplementary material (section S4). In phase two, the behaviour of

161   N_2O emissions and dissolved N_2O concentration during normal operation was investigated;

162   efforts were focused to identify dependencies with the operational dataset and laboratory

163   analyses. Finally, in phase three, classification and regression models were trained to predict the

164   behaviour of aerobic dissolved N_2O concentration in the different cycles. A support vector

165   machine classification (SVM) and regression (SVR) models were constructed (Cortes and

166   Vapnik, 1995).

167   The first step for the prediction of the average aerobic dissolved N_2O concentration included the

168   training of an SVM classifier (ANOXSVM) to predict whether dissolved N_2O will be consumed

169   during the anoxic phase. This was significant, given that accumulated dissolved N_2O in the

170   beginning of the aerobic phase, will be stripped during aeration. All cycles were divided in two

171   classes: class anoxA (dissolved N_2O < 0.6 mg/L) and class anoxB (dissolved N_2O > 0.6 mg/L).

172   The dissolved N_2O concentration threshold was set equal to 0.6 mg/L, since in ~88% of these

173   cases, N_2O was consumed by the end of subsequent anaerobic phase. In cycles belonging to class

174   anoxA, no N_2O carryover was assumed. It is important to note that the term anaerobic phase, is

                                          8

175 used to describe the first operational phase of the SBR (Figure 1) within each cycle and is not

176 necessarily representative of the actual conditions in the reactor.

177 Subsequently, an SVM classifier (ANSVM) was trained to predict if dissolved N_2O will be

178 consumed in the subsequent anaerobic phase. The threshold of N_2O at the end of the anaerobic

179 phase was set equal to 2.6 mg/L (sensor calibration limit). Therefore, anaerobic phases with

180 accumulated N_2O were classified in two groups: class anaerA (N_2O concentration < 2.6 mg/L)

181 and anaerB (N_2O concentration > 2.6 mg/L) . Cycles belonging to anaerA class, were used to

182 train an SVR model (ANSVR) to predict the dissolved N_2O concentration at the end of the

183 anaerobic phase.

184 Finally, an SVR model was trained to predict the average N_2O concentration during the aerobic

185 phase (AERSVR), utilizing the ANSVR model predictions for cycles with initial aerobic N_2O less

186 than 2.6 mg/L. Finally, the aerobic SVR model was also tested to cycles belonging in class

187 anaerB (N_2O concentration > 2.6 mg/L). In anaerB cycles, initial aerobic N_2O accumulation

188 exceeds the calibration limit of the sensor. Additionally, aerobic N_2O accumulation starts before

189 completion of the stripping of pre-existing dissolved N_2O. In these cases, the average dissolved

190 N_2O concentration of the cycle, was calculated considering the period from the first minimum of

191 dissolved N_2O concentration until the end of aeration (or after 30 min if a local minimum did not

192 exist). Additionally, initial N_2O accumulation was assumed to be equal to 0.6 mg/L (average

193 minimum after initial N_2O stripping observed in these cycles).

194   In practice, the methodology followed was not linear as it is illustrated in Figure 2; it involves

195 several backward and forward loops between the different steps. The feedback loops were

196 necessary to leverage the knowledge discovered and adjust the data-preparation (i.e. new features

197 extraction, different pre-processing) and mining phases.

9

198   [Figure 2]

199   2.2.1   *Support Vector Machines classification and Support vector regression*

200   Support vector machines (SVMs) are a range of supervised non-parametric classification and

201   regression algorithms that have various applications in several fields including hydrology

202   (Raghavendra and Deka, 2014), bioinformatics (Byvatov and Schneider, 2003) and wastewater

203   (Corominas et al., 2018). For instance, in wastewater, support vector regression (SVR) has been

204   successfully applied to data generated from mechanistic modelling of biological processes (Fang

205   et al., 2011) or to experimental data (Seshan et al., 2014) to predict reactors' performance.

206   SVM classification and SVR models were constructed to predict the behaviour of dissolved N_2O

207   production/consumption in different phases of the SBR operation (Figure 2). SVM aims to define

208   an optimum separating hyperplane in the feature space that maximizes the margin between two

209   different classes. Classes with large margins are clearly separable and provide a 'safety' for the

210   generalisation of the algorithm when applied to new points. In practical applications, the

211   overlapping of a number of data belonging to the two classes, is common. Therefore, soft margins

212   are introduced to allow a number of misclassifications to identify feasible solutions when the

213   training dataset is not strictly linearly separable. Similarly, in the SVR case, the aim of the

214   method is to identify the hyperplane that has the minimum distance to all data points. A complete

215   description of the SVM and SVR algorithms is provided in the supplementary material. Radial

216   basis function (RBF) was selected to construct the models in this study. The 'kernel trick' and

217   enables SVMs to operate even in infinite feature space (where data are mapped), without in

218   practice executing calculations there (Luts et al., 2010).

219   The algorithms were implemented with the kernlab package (Karatzoglou et al., 2004) in R

220   software. Repeated 10-fold cross validation (3 repetitions) was applied to select the cost and

10

221   gamma (γ) regularization parameters over a grid-search with the caret package (Kuhn, 2008). The

222   cost determines the penalty of misclassified instances or instances violating the maximal margin

223   whereas γ determines the amplitude of the kernel. The dataset was randomly divided into test and

224   train, with 70% of the available data used for training the SVM model and 30% used for testing.

225   In the classification case, over-sampling was applied for the minority classes within the 10-fold

226   cross validation loop (before training). Local models were developed based on observations from

227   each phase of the SBR reactor instead of the dataset from the duration of the whole cycle. The

228   underlying characteristics and dependencies of the operational variables vary between anoxic,

229   aerobic and anaerobic conditions. Additionally, the performance of the system under different

230   phases within the cycle can also vary. There are significant benefits in the development of local

231   phase-based models. The behaviour of dissolved N_2O and triggering operational conditions vary

232   between the different phases; local models enable to investigate the phase-based dependency

233   structures that would not be possible using the whole cycle dataset. The performance of the

234   classification SVM models were evaluated based on accuracy and kappa and from the sensitivity

235   and specificity as described in the supplementary material (S3.1). Similarly, the regression

236   models were evaluated considering the root mean squared error (RMSE) and R-squared (R^2)

237   (S3.1).

238   **3.   Results and discussion**

239   **3.1   SCENA performance**

240   The SBR treats up to 43 kg of N/day of anaerobic supernatant, which results in a volumetric

241   nitrogen loading rate up to 0.78 kgN/m^3 day. The performance of the SBR reactor in terms of

242   NH_4-N removal, was stable during the monitoring campaign. During system's normal operation

243   (January 2019 - April 2019), the average removal efficiency of NH_4-N, TN and PO_4-P was 78%,

11

244 ~77% and 84% respectively. Influent and effluent concentrations of the SCENA system for the

245 duration of the monitoring campaign are provided in Table 1. A detailed description of the

246 abnormal cycles isolated is provided in the supplementary material

247 [Table 1]

248 **3.2 N$_2$O Emission factor**

249 N$_2$O emissions were measured using a gas analyser (March – April 2019); on average ~0.8 kg of

250 N$_2$O-N was emitted in each cycle, equivalent to 7.6% of the NH$_4$-N load in the SBRR. In terms

251 of the NH$_4$-N removed the N$_2$O EF was equal to 11% ($\pm$4). The emissions during the aerobic

252 phase were considered. N$_2$O emissions exhibited significant variability ranging from 0.14 kg

253 N$_2$O-N/cycle (1.3% of NH$_4$-N load) to ~2 kg N$_2$O-N/cycle (19% of NH$_4$-N load) as shown in

254 Figure 3 (a). Emission peaks higher than 1.5 kg N$_2$O-N/cycle and the increasing trend observed

255 close to the end of the monitoring campaign coincide with peaks in the conductivity change in the

256 aerobic phase of the cycles (Figure 3 (b)). Laboratory analyses performed approximately four

257 times per week, did not demonstrate any significant changes in the influent COD, NH$_4$-N loads

258 and removal efficiencies linked with the increasing trend of the emissions observed in Figure 3

259 (a). Given the wide range of the N$_2$O emissions observed in the system, in the following sections,

260 efforts were focused to identify triggering operational conditions.

261 [Figure 3]

262 **3.3 Energy consumption vs N$_2$O emissions**

263 The operational carbon footprint of the sidestream line was estimated using the direct GHG

264 emissions (from N$_2$O) and electricity consumption. The electricity consumption was relatively

265 steady over the monitoring period; on average ~5.4 kWh was consumed in the SBR for the

266 removal of 1 kg of NH$_4$-N from the anaerobic supernatant. The average energy consumption of

the SBR represented ~77% of the total electricity consumption of the SCENA system. On average ~48.7 kg of CO_{2eq} are generated for the removal of 1 kg of NH_4-N due to the direct N_2O emissions and electricity consumption in the system. The contribution of the total N_2O emissions to the operational carbon footprint of the S.C.E.N.A process ranged from 66.7% to 96.8% when all the equipment electricity consumption (i.e. fermenter, dynamic thickener) were considered. Given the variability of the N_2O emissions observed in the system (Figure 3) the kg of CO_{2eq} emitted per kg of NH_4-N removed ranged between 9.5 kg CO_{2eq} to 117.7 kg CO_{2eq}. Figure 4 (a), shows the average operational carbon footprint (considering direct N_2O emissions and electricity consumption) of the SCENA system for two cases with different ranges of N_2O emissions. In the first case (26/03), a considerable amount of N_2O was emitted, equal to ~10.5% of the influent NH_4-N load. In the second case, the emissions were significantly lower, equal to ~4% of the influent NH_4-N load. Both cases are characterised by similar influent NH_4-N concentrations, phase duration, temperature and ammonia removal efficiencies (~79%). The DO concentration is equal to ~1 mg/L. In case 1, the operational carbon footprint of the process is ~136% higher compared to case 2. This example shows that under similar conditions (considering laboratory analyses, average pH and DO), dissolved N_2O concentrations can vary significantly in the studied system. Investigation of the behaviour of conductivity during the two aerobic phases, showed higher conductivity and pH decrease in case one (~ 510 μS/cm and ~1 respectively) compared to case two (~350 μS/cm and 0.7 respectively) (Figure 4 (b) and (c)). Additionally, the initial aerobic ORP in case 2, was higher (-43 mV) compared to case 1 (-274 mV) (Figure 4 (b)). Therefore, efforts to understand the N_2O triggering operational conditions and mitigate GHG emissions, should consider the dynamic in-cycle behaviour of the variables monitored in the system. The relationship between the operational variables (i.e. DO, NH_4-N concentration, ORP, conductivity) will be discussed in the following sections.

13

291   [Figure 4]

292   **3.4   Variability of N_2O emissions during normal operation**

293   N_2O was emitted during aeration phase in all cycles and correlated significantly with the

294   dissolved N_2O accumulation.   One representative cycle profile for the dissolved N_2O

295   concentration and N_2O emissions in cycles starting without dissolved N_2O accumulation from the

296   previous cycle is shown in Figure 5, together with the DO, NH_4-N, conductivity, ORP and pH.

297   ORP at the beginning of the aerobic phase shows a correlation with the DO, whereas N_2O

298   accumulation is minimum. Dissolved N_2O increases in the first 60-70 min of aeration (a small

299   change in the pH slope can be seen coinciding with the peak of accumulated N_2O) indicating that

300   the generated N_2O generation is higher than the stripped N_2O. N_2O accumulation shows a

301   decreasing trend after ~90 minutes of aeration. Subsequently dissolved N_2O concentration

302   increases when aeration stops, and the anoxic phase starts. This shows that production of N_2O

303   continues under decreasing DO and until DO depletion. The calibration range of the dissolved

304   N_2O probe is between 0 - 2.6 mg/L. Therefore, the accumulation of dissolved N_2O can be higher

305   than the peak shown in Figure 5. During the anoxic phase, pH increases rapidly during the dosage

306   of fermentation liquid, followed by a slow decrease upon the end of carbon dosage phase. A

307   sudden change in the ORP signal slope ('nitrite knee') indicates the depletion of nitrite whereas

308   TN still exists in the form of N_2O. Accumulated N_2O is subsequently depleted rapidly after NO_2^-

309   N depletion.

310   [Figure 5]

14

311   **3.5   The pattern of N_2O emissions**

312   Offline data from laboratory studies and the ranges of the operational variables were analysed in

313   order to investigate significant changes that contribute to high accumulation of dissolved N_2O

314   concentration and high N_2O emissions.

315   Figure 6 (a) shows the daily average dissolved N_2O concentration (coloured points) during

316   aerobic phase versus conductivity at the end of aerobic phase and the effluent NH_4-N

317   concentration. Conductivity is significantly related and can be linked with the NH_4-N

318   concentration in the reactor (spearman correlation coefficient equal to 0.97). High average

319   aerobic dissolved N_2O concentration (>1.5 mg/L) was mainly observed with NH_4-N

320   concentrations lower than 150 mg/L and higher than 300 mg/L in the effluent of the SBR.

321   Additionally, the spearman correlation coefficient between dissolved N_2O and average aerobic

322   conductivity decrease rate (μS/cm/min) was equal to -0.7 and N_2O concentration peaks were

323   observed for conductivity decrease rate > 1.8 μS/cm/min. The latter indicates that higher

324   emissions occur under high ammonia removal efficiency that can be linked with higher ammonia

325   oxidation rates (AOR) (i.e. due to pH values observed ~ 8) triggering the NH_2OH oxidation

326   pathway or higher than average NO_2^-N accumulation (triggering nitrifier denitrification

327   pathway). Domingo-Félez et al., (2014) found that N_2O production rates were positively

328   correlated with the extant nitrification rate in a single-stage nitritation/Anammox reactor.

329   Similarly, Law et al. (2011) identified a linear relationship between AOR and N_2O emissions in a

330   partial nitration SBR reactor treating the reject water from anaerobic digestion. Law et al. (2011)

331   suggested that is attributed to higher accumulation of the ammonium oxidation intermediates

332   (hydroxylamine (NH_2OH) and nitrosyl radical (NOH)) leading to faster N_2O formation or to the

333   increased use of electrons reducing nitrite to nitric oxide (nitrifier denitrification pathway) under

334   low DO concentrations. High nitrite accumulation has been also linked with elevated N_2O

15

335 emissions and the nitrifier denitrification pathway, especially under low DO concentrations

336 (Tallec et al., 2006; Kampschreur et al., 2008; Desloover et al., 2011; Peng et al., 2015; Massara

337 et al., 2017; Law et al., 2012). For instance, Peng et al. (2017) and Kampschreur et al. (2009), in a

338 nitritation-denitritation SBR and a full-scale single stage nitritation-Anammox reactor

339 respectively, identified linear relationship between nitrite accumulation and N_2O emissions at

340 DO levels below 1.5 mg/L. Similarly, Tallec et al (2006) in a nitrifying activated sludge observed

341 eightfold increase of N_2O emissions with the addition of nitrite pulses (10 mg/L) at DO equal to 1

342 mg/L. Therefore, both hydroxylamine oxidation and the nitrifier denitrification are possible

343 during aeration in the investigated SBR.

344 The average dissolved N_2O concentration during the aerobic phase of different cycles varied

345 significantly in relation to the average DO concentration. Figure 6 (b), shows that the dissolved

346 N_2O concentration peaks coincided with average DO concentrations less than 0.9 to 1 mg/L. The

347 spearman correlation coefficient between dissolved N_2O and DO concentrations was equal to -

348 0.7. The coloured points in the Figure, represent the ORP at the end of the aerobic phase; ORP is

349 higher than 40 mV in the majority of the cycles with average aerobic dissolved N_2O

350 concentration less than 1 mg/L. Only cycles without dissolved N_2O accumulation from the

351 previous anoxic phase are shown in the graph. Stenström et al. (2014) showed decreasing DO

352 concentrations lower than 1–1.5 mg/L are linked with higher nitrite accumulation and are

353 positively correlated with N_2O emissions during nitrification in a full-scale predenitrification-

354 nitrification SBR treating anaerobic supernatant. Similarly, Pijuan et al., (2014) reported an

355 increase of N_2O emissions in a nitritation reactor with the reduction of DO from 4 to <1 mg/L.

356 During the monitoring period, blowers operated at maximum flow-rate. Therefore, the presence

357 of residual biodegradable COD concentration in the aerobic, is expected to decrease DO

358 concentration. Similarly, higher influent NH_4^+ loads or higher ammonia oxidation rates (that can

16

359   also result in increased NO_2^- accumulation) can impact the DO concentration in the system. The

360   dissolved N_2O concentration can be affected by a combination of variables; therefore, it cannot be

361   deduced that the decreased DO is the sole contributing factor triggering the increased N_2O

362   generation observed.

363   [Figure 6]

364   3.6   Impact of accumulated N_2O in the end of anoxic and anaerobic phase

365   Several parameters have been reported to affect the N_2O accumulation under anoxic conditions,

366   such as the inhibition of the nitrous oxide reductase (Nos) by free nitrous acid (FNA) or high

367   accumulation of NO_2^-, the electron competition between electro acceptors and the type of carbon

368   source (Itokawa et al., 2001; Pan et al., 2013; Zhou et al., 2008; Zhu and Chen, 2011).

369   Additionally, low values of COD/N can result in incomplete denitritation and therefore, N_2O

370   accumulation via the heterotrophic denitrification pathway during the anoxic phase of the SBR.

371   Accumulated N_2O in the end of the anoxic phase is stripped in the subsequent cycle, increasing

372   the N_2O emissions. Caranto et al. (2016) have recently showed that N_2O can be the main product

373   of anaerobic NH_2OH oxidation catalysed by the cytochrome P460 in N. europaea. The latter can

374   be an evidence of the biological N_2O generation under limited DO and high NH_3 concentrations,

375   both conditions occurring in the target system in the during the transition from aerobic to anoxic

376   phases when N_2O accumulation rapidly increases.

377   In this study, the average soluble COD concentration in the fermentation liquid was equal to

378   13082 mg COD/L over the monitoring period (Table 1). Overall, in >27% of the examined cycles

379   the N_2O was completely consumed by the end of the anoxic phase. Zhu and Chen, (2011),

380   showed that the use of sludge alkaline fermentation as carbon source in an anaerobic-aerobic

381   system treating high-strength stream, can reduce the N_2O production by up to 68.7% compared to

382 alternative carbon sources (i.e. acetic acid). On the other hand, Li et al., (2013a) in a process

383 utilizing PHA as internal carbon source, observed higher N_2O production and reduction rates at

384 higher influent COD concentrations linked with higher anaerobic PHA synthesis (ranging from

385 100 to 500 mg/L). The higher N_2O production rates were attributed to the accumulated NO_2^-

386 inhibiting the N_2O reduction.

387 The dissolved N_2O concentration in the anoxic phase exceeded the calibration limit of the

388 sensors; only cycles in which "nitrite knee" was observed and N_2O reduced to values lower than

389 2.6 mg/L could be investigated. Therefore, the effect on NO_2^- in anoxic N_2O generation could not

390 be studied. However, studies have shown that elevated NO_2^- concentrations during denitrification

391 can reduce the denitrification rate and increase the N_2O accumulation (Schulthess et al., 1995).

392 The electron competition between nitrite reductase NIR, nitric oxide reductase (NOR) and nitrous

393 oxide reductace (NOS) is intensified under high NO_2^- concentrations; NOS is less competitive

394 under limitation of electron donor and this will result in N_2O accumulation (Pan et al., 2013; Ren

395 et al., 2019).

396 Based on the profiles shown in Figure 5 , N_2O was always consumed after the depletion of NO_2^-

397 during denitritation; specifically, dissolved N_2O concentration decreased after the "nitrite knee".

398 Gabarró et al. (2014), studied a partial-nitritation reactor treating landfill leachate, and operated

399 under alternating aerobic/anoxic conditions to allow heterotrophic denitritation. The authors

400 demonstrated that significant N_2O accumulation was observed during anoxic periods. NO_2^-

401 denitrification rate was higher under both biodegradable COD limiting conditions and after

402 acetate addition compared to N_2O reduction; N_2O reduction rate was maximum after NO_2^-

403 removal (similar to what was observed in this study). In denitrifying phosphorus removal

404 processes, Li et al. (2013) showed that the N_2O accumulation can be higher compared to

405 conventional denitrification; the authors suggested that in the electron competition between

18

406 denitrifying enzymes and PHA, N_2O reductase is less competitive. On the other hand, Ribera-

407 Guardia et al. (2016) investigated the electron competition during denitrification (PHA as the sole

408 carbon source) of enriched dPAO and dGAO biomass and found that higher N_2O accumulation

409 in the latter culture. Additionally, the last step of denitrification was inhibited in dGAO cultures (

410 N_2O accumulation up to ~84% of the N-reduced), under high levels of NO_2^- (~ 15 mgN/gVSS)

411 whereas N_2O consumption in dPAO biomass was not affected. Wang et al., (2015) demonstrated

412 that during denitrifying phosphorus removal, mitigation of NO_2^- accumulation is possible via

413 continuous dosage of phosphate and nitrate. Wang et al., (2011), showed that optimisation of the

414 synthesis of PHA during the anaerobic phase can mitigate the N_2O production during the anoxic

415 phase leading to complete denitrification.

416 In the system, N_2O emissions and dissolved N_2O concentration at the aerobic phase is strongly

417 related with incomplete denitritation in the previous cycle. In ~26% of the cycles with incomplete

418 denitritation, the N_2O concentration did not decrease below ~2 mg/L in the anaerobic phase and

419 therefore the stripping of accumulated N_2O in the subsequent aerobic phase was substantial.

420 Figure 7 (a) shows representative profiles of the dissolved N_2O concentration and the N_2O

421 emissions based on different initial concentrations of N_2O in the beginning of the aerobic phase.

422 The profiles of the ORP, DO and pH are comparable in the preseted cycles (Figure 7 (b)). In

423 cycle B ~0.56 kgN of N_2O were emitted during the aerobic phase, wheareas in cycle A N_2O

424 emissions are equal to 0.33 kgN (given the duration of these cycles is not equal only 220 min

425 were considered). The initial dissolved N_2O concentration in cycles A and B is equal to 0.27 and

426 >2.6 mg/L respectively. The N_2O emissions increased significantly due to the accumulated N_2O

427 at the beginning of the previous anoxic phase that was stripped at the beginning of aeration.

428 Overall, in ~72% of the cycles, the dissolved N_2O concentration at the beginning of the anaerobic

429 phase was higher than 0.3 mg/L. In cycles with dissolved N_2O concentration higher than 0.3

430   mg/L at the beginning of the anaerobic phase, the change in dissolved N_2O concentration during

431   the anaerobic phase was highly correlated with the ORP at the beginning of the anaerobic phase.

432   Additionally, the spearman correlation coefficient between the magnitude of the ORP reduction

433   and magnitude of the dissolved N_2O reduction was equal to 0.7. Figure 8 shows the boxplots of

434   dissolved N_2O reduction in relation to initial anaerobic ORP and ORP change for two cases: i)

435   negligible dissolved N_2O change mainly due to influent dilution or anaerobic dissolved N2O

436   concentration > 2.6 mg/L, and ii) occasions with N_2O reduction during the anaerobic phase. In

437   Figure 8 (a) only occassions with ORP decrease higher than -50 mV are shown. The presence of

438   nitrites in the bulk liquid during the (anaerobic) phase affected the ORP. NO_2-N depletion in the

439   bulk liquid resulted in a sharp "nitrite knee" in the ORP profile (similar to the one observed

440   during the anoxic phase. Therefore, higher ORP change was expected in cycles with NO_2-N

441   depletion and N_2O consumption during the anaerobic phase.

442

443   [Figure 7]

444   Anaerobic phase term, is used to describe the first operational phase of the SBR (Figure 1) within

445   each cycle and might not represent the actual conditions in the reactor. For instance, ORP ~ -80

446   mV in the anaerobic phase of the SBR indicates anoxic conditions, due to residual NO_2^-N

447   concentration from the previous anoxic phase of the reactor.

448   [Figure 8]

449   **3.7   Prediction and control of N_2O accumulation in the anoxic and anaerobic phases**

450   As discussed in section 3.6, the behaviour of ORP was significantly related with the behaviour of

451   NO_2^- and consequentially of the dissolved N_2O concentration during the anaerobic phase.

452   Therefore, in the ANSVM model, features related with the ORP profile were mainly used (Table

453   2). Similarly, there was a strong link with the ORP behaviour and the nitrite "knee" with the N_2O

454   accumulation during the anoxic phase. The features considered in ANOXSVM model are shown

455   in Table 2.

456   [Table 2]

457   The classification matrices for train and test datasets of the ANSVM and ANOXSVM models are

458   presented in Table 3. The average classification accuracy for the ANOXSVM model, was equal

459   to 99% and 97% for the test and validation datasets. Similar results were obtained for the

460   anaerobic phase with 95% and 98% accuracy in the train and test datasets respectively.

461   Jaramillo et al. (2018) developed an SVM classifier to estimate online the end of partial

462   nitrification in a laboratory aerobic-anoxic SBR based on features extracted from pH and DO

463   sensors over time-windows, resulting in 7.52% reduction in the operational time. In this study, the

464   main focus was to estimate offline the behaviour of N_2O emissions based on historical batch data.

465   The results from this study indicate that ORP and pH sensor data can be used to detect the

466   consumption of N_2O during the nitritation/nitrification in SBR reactors. The results show that

467   knowledge-based feature-extraction and SVM classification could help in explaining the

468   behaviour of the system and potentially optimise the control to consider the consumption of

469   accumulated N_2O (i.e. in this system the denitritation can be stopped after the local maximum of

470   the ORP rate after the nitrite "knee" in all the cycles investigated.)

471   [Table 3]

472   Figures 9 (a) and (b) illustrate the predicted and measured N_2O concentration at the end of the

473   anaerobic phase (ANSVR model). The SVR parameters were optimised based on the root mean

474   square error using the train dataset. RMSE of the SVR model was equal to 0.11 and 0.1 mg N_2O-

475   N/L for the train and test datasets respectively (R-squared equal to 0.85 and 0.75 respectively).

476   As shown in Figure 9 (b) the simulation results follow the behaviour of the actual dissolved N_2O

477   concentrations observed. One of the major factors affecting the performance is the limited

478   number of data points, but the prediction is still accurate.

479   [Figure 9]

480   **3.8   Prediction of the N_2O concentration in aerobic phase**

481   The input features are shown in Table 4 and were selected based on the identified influential

482   variables. The N_2O predicted values of the ANSVR model were used (anaerP). The procedure

483   followed for the selection of model parameters was similar to the respective one followed for the

484   anaerobic phase. Additionally, ANSVR test dataset cycles, were identified and used in AERSVR

485   test dataset A. The model was also applied in anaerB cycles (test dataset B).

486   [Table 4]

487   Figure 10 (a), shows the predicted and measured average aerobic N_2O concentration for the

488   trained and test datasets. RMSE of the SVR model was equal to 0.06 and 0.11 mg N_2O-N /L for

489   the train dataset and test dataset A respectively, whereas the R-squared was equal to 0.94 and

490   0.82 (Figure 10 (a) and (b)).

491   [Figure 10]

492   The RMSE of the predicted values for the test dataset B, was equal to 0.29 mg N_2O-N/L and the

493   R-squared was equal to 0.72 (Figure 10 (a)). The AERSVR model underpredicted the average

494   dissolved N_2O concentration of test B dataset. This is expected given that in test B dataset cycles,

495   the initial aerobic N_2O accumulation exceeds the sensor calibration limit. Therefore, on many

496   occasions the initial aerobic N2O accumulation was also underestimated (section 2.2.1 - anaerB

497   cycles). An example is shown if Figure 11. In cycle A, the average dissolved N_2O concentration

498   (calculated as discussed in section 2.2.1 for anaerB cycles) is equal to 1.33 mg/L. The AERSVR

499   model predicted 0.87 mg/L underestimating the actual concentration (considering initial

500   accumulation equal to 0.6 mg/L). In cycle B, the AERSVR model predicted N_2O concentration

501   equal to 0.61 mg/L (considering initial accumulation equal to 0.6); the observed average

502   dissolved N_2O concentration (after the local minimum), was equal to 0.6 mg/L.

503   [Figure 11]

504   The results show that under the investigated operational conditions, the framework shown in

505   Figure 2**Error! Reference source not found.** can provide a good estimation of the real dissolved

506   N_2O behaviour and concentration observed during the different phases of SBR operation.

507   Instabilities in the performance of machine learning models due to changes in the operational

508   conditions in wastewater bioreactors have been reported in the literature (Shi and Xu, 2018).

509   Therefore, long-term datasets and investigation of different patterns and dependencies should be

510   investigated before model construction.

511   **3.9   Mitigation strategy**

512   During aerobic phases, elevated average dissolved N_2O concentration was linked with DO less

513   than 1 mg/L and increased conductivity decrease rates (conductivity values represent NH_4-N

514   concentration values in the reactor). Therefore, cycles with increased conductivity decrease rate

515   indicate higher NH_4-N removal efficiency and NO_2^-N accumulation. Dissolved N_2O

516   concentrations lower than 0.6 mg/L were identified in cycles with average DO concentration

517   equal to ~1.36 mg/L, and conductivity decrease rate > 1.8 μS/cm/min. Increasing the reactor DO

518   concentration to values higher than 1.3 mg/L can result in decreased aerobic N_2O generation

519   (Law et al., 2012). However, with the current anaerobic supernatant feeding strategy, blowers

520   operate at maximum flowrate, so it is not possible to increase the aeration in the system.

521   On the other hand, the implementation of a step-feeding strategy could foster the reduction of

522   N_2O emissions thanks to the lower NH_4-N and free ammonia (FA) concentration at the beginning

523   of the cycle, which has been recognized as a triggering factor for N_2O production (Desloover et

524   al., 2012). Conductivity at the end of the cycle can act as surrogate to estimate the effluent NH_4-N

525   concentration of the reactor and optimize the anaerobic supernatant feeding load. Consequently,

526   the aerobic initial NH_4-N concentration could be controlled to avoid either FA accumulation or

527   high AOR with subsequent N_2O generation.

528   Additionally, frequent alternation of aerobic/anoxic phases can be introduced in order to avoid

529   high nitrite accumulation. The impact of nitrite concentration on N_2O production can be also

530   minimized by ensuring adequate DO levels within the reactor to inhibit the nitrifiers

531   denitrification pathway (Blum et al., 2018; Law et al., 2013). Rodriguez-Caballero et al. (2015)

532   reported that in a full-scale SBR treating municipal wastewater, intermittent aeration (alternation

533   between 20–30 min oxic and anoxic) led to a minimization of N_2O compared to long oxic periods

534   that enhanced N_2O emission. The authors related this behaviour to the presence of shorter

535   aeration times with subsequently lower nitrite accumulation and N_2O production.

536   In addition, Su et al. (2019) reported that slightly acidic or neutral pH in nitration reactors (at

537   values that do not inhibit microbial activity) can decrease N_2O generation by up to seven times.

538   Based on the pH profiles observed in this study, regulation of aerobic (alkalinity consumption)

539   phase duration can be also considered to control the pH at lower levels.

540   The developed models can be used to estimate rapidly and precisely the hard-to-measure N_2O

541   concentrations during aeration and detect N_2O accumulation in non-aerated phases. Additionally,

542   it can alert operators about cycles with anoxic and anaerobic N_2O accumulation and elevated

543   aerobic N_2O concentrations, that require modifications to the system operation. The ANOXSVM

544   model can predict if N_2O is consumed in anoxic phases or if anoxic duration should be extended.

545   Thus, additional provision of fermentation liquid can be performed to promote N_2O consumption

546   through denitritation, when after 70-90 minutes the anoxic SVM model still indicates incomplete

547   denitritation.

548   This study provides evidence on the relationship of DO, ORP and conductivity and pH with the

549   dissolved N_2O concentration (in terms of correlation coefficients, behaviour and thresholds that

550   indicate specific ranges of N_2O accumulation). These findings together with the models

551   developed in this study, can be the basis for the development of intelligent control algorithms to

552   integrate emissions control in sidestream SBR reactors performing nitritation/partial nitritation or

553   other systems similar to S.C.E.N.A. Moreover, features based on ORP, pH, DO and conductivity

554   measurements in wastewater SBR processes, that can be used to predict dissolved N_2O

555   concentrations have been identified. The developed framework can be also tested in continuous

556   processes for the data-driven prediction of N_2O emissions.

557   **Conclusions**

558   Knowledge discovery and data-mining techniques were employed to extract useful information

559   about the dynamic behaviour of N_2O, and to predict the behaviour of dissolved N_2O concentration

560   in a full-scale SBR reactor treating the anaerobic supernatant. The main conclusions are

561   summarized as follows:

562   • The N_2O emissions in SCENA process varies from 1.3% to 19% of NH_4-N load,

563   therefore they can contribute considerably to the operational carbon footprint of the

564   process (~90% on average).

565   • Average aerobic dissolved N_2O concentration could significantly under similar influent

566   loads, DO, pH and removal efficiencies. Extracting information from the dynamic in-

567   cycle behaviour of the variables monitored in the system is a significant step towards

568   understanding N_2O behaviour.

569   • Aerobic dissolved N_2O concentration peaks (>1 mg/L), were observed in cycles with

570   average DO concentrations less than 0.9-1 mg/L and ORP concentration at the end of the

571   aerobic phase less than 40 mV. Conductivity was correlated with the reactor NH_4-N

572   concentration (0.97). N_2O peaks were also observed in cycles with elevated decrease of

573   conductivity during aeration. Step-feeding, control of initial NH_4-N concentrations and

574   control of pH via the regulation of aerobic phase duration can mitigate the N_2O peaks

575   observed in this study.

576   • The accumulation of N_2O at the end of the SBR anoxic phase was stripped in the

577   subsequent aerobic phase and had a significant impact on the amount of N_2O emitted.

578   The accumulated N_2O was consumed rapidly after nitrite 'knee' that was linked with the

579   nitrite depletion. The ANOXSVM model can be used to detect if anoxic duration should

580   be extended or additional fermentation liquid provided to enhance N_2O consumption in

581   anoxic phases.

582   • This study shows that low-cost sensors, conventionally used to monitor SBR systems (i.e.

583   pH, DO, ORP), have good capabilities to predict the dissolved N_2O behaviour and

584   concentrations when couple with knowledge discovery techniques. The AERSVR model,

585   showed reliable estimations of the aerobic N_2O concentration and can provide guidance

586   to WWTPs operators, on whether N_2O levels are acceptable or mitigation actions are

587   required.

588   **Acknowledgements**

591 **References**

592 Blum, J.-M., Jensen, M.M., Smets, B.F., 2018. Nitrous oxide production in intermittently aerated

593 Partial Nitritation-Anammox reactor: oxic N2O production dominates and relates with ammonia

594 removal rate. Chem. Eng. J. 335, 458–466. https://doi.org/10.1016/j.cej.2017.10.146

595 Byvatov, E., Schneider, G., 2003. Support vector machine applications in bioinformatics. Appl.

596 Bioinformatics 2, 67–77.

597 Caranto, J.D., Vilbert, A.C., Lancaster, K.M., 2016. Nitrosomonas europaea cytochrome P460 is

598 a direct link between nitrification and nitrous oxide emission. Proc. Natl. Acad. Sci. 113, 14704–

599 14709. https://doi.org/10.1073/pnas.1611051113

600 Corominas, Ll., Garrido-Baserba, M., Villez, K., Olsson, G., Cortés, U., Poch, M., 2018a.

601 Transforming data into knowledge for improved wastewater treatment operation: A critical

602 review of techniques. Environ. Model. Softw., Special Issue on Environmental Data Science.

603 Applications to Air quality and Water cycle 106, 89–103.

604 https://doi.org/10.1016/j.envsoft.2017.11.023

605 Cortes, C., Vapnik, V., 1995. Support-vector networks. Mach. Learn. 20, 273–297.

606 https://doi.org/10.1007/BF00994018

607 Desloover, J., De Clippeleir, H., Boeckx, P., Du Laing, G., Colsen, J., Verstraete, W., Vlaeminck,

608 S.E., 2011. Floc-based sequential partial nitration and anammox at full scale with contrasting

609 N2O emissions. Water Res. 45, 2811–2821. https://doi.org/10.1016/j.watres.2011.02.028

610 Desloover, J., Vlaeminck, S.E., Clauwaert, P., Verstraete, W., Boon, N., 2012. Strategies to

611 mitigate N2O emissions from biological nitrogen removal systems. Curr. Opin. Biotechnol.,

612 Energy biotechnology • Environmental biotechnology 23, 474–482.

613 https://doi.org/10.1016/j.copbio.2011.12.030

28

614 Domingo-Félez, C., Mutlu, A.G., Jensen, M.M., Smets, B.F., 2014. Aeration Strategies To

615 Mitigate Nitrous Oxide Emissions from Single-Stage Nitritation/Anammox Reactors. Environ.

616 Sci. Technol. 48, 8679–8687. https://doi.org/10.1021/es501819n

617 Eskicioglu, C., Galvagno, G., Cimon, C., 2018. Approaches and processes for ammonia removal

618 from side-streams of municipal effluent treatment plants. Bioresour. Technol. 268, 797–810.

619 https://doi.org/10.1016/j.biortech.2018.07.020

620 Ester, M., Kriegel, H.-P., Sander, J., Xu, X., 1996. A density-based algorithm for discovering

621 clusters in large spatial databases with noise., in: Kdd. pp. 226–231.

622 Fang, F., Ni, B., Li, W., Sheng, G., Yu, H., 2011. A simulation-based integrated approach to

623 optimize the biological nutrient removal process in a full-scale wastewater treatment plant. Chem.

624 Eng. J. 174, 635–643. https://doi.org/10.1016/j.cej.2011.09.079

625 Frison, N., Katsou, E., Malamis, S., Oehmen, A., Fatone, F., 2015. Development of a novel

626 process integrating the treatment of sludge reject water and the production of

627 polyhydroxyalkanoates (PHAs). Environ. Sci. Technol. 49, 10877–10885.

628 Gabarró, J., González-Cárcamo, P., Ruscalleda, M., Ganigué, R., Gich, F., Balaguer, M.D.,

629 Colprim, J., 2014. Anoxic phases are the main N2O contributor in partial nitritation reactors

630 treating high nitrogen loads with alternate aeration. Bioresour. Technol. 163, 92–99.

631 https://doi.org/10.1016/j.biortech.2014.04.019

632 Haimi, H., Mulas, M., Corona, F., Vahala, R., 2013. Data-derived soft-sensors for biological

633 wastewater treatment plants: An overview. Environ. Model. Softw. 47, 88–107.

634 https://doi.org/10.1016/j.envsoft.2013.05.009

635 IPCC, 2013. The physical science basis. Contribution of working group I to the fifth assessment

636 report of the intergovernmental panel on climate change. USA: Cambridge University Press.

637 Itokawa, H., Hanaki, K., Matsuo, T., 2001. Nitrous oxide production in high-loading biological

638 nitrogen removal process under low cod/n ratio condition. Water Res. 35, 657–664.

639 https://doi.org/10.1016/S0043-1354(00)00309-2

640 Janus, H.M., van der Roest, H.F., 1997. Don't reject the idea of treating reject water. Water Sci.

641 Technol. 35, 27–34. https://doi.org/10.2166/wst.1997.0351

642 Jaramillo, F., Orchard, M., Muñoz, C., Antileo, C., Sáez, D., Espinoza, P., 2018. On-line

643 estimation of the aerobic phase length for partial nitrification processes in SBR based on features

644 extraction   and   SVM   classification.   Chem.   Eng.   J.   331,   114–123.

645 https://doi.org/10.1016/j.cej.2017.07.185

646 Kampschreur, M.J., Poldermans, R., Kleerebezem, R., Star, W.R.L. van der, Haarhuis, R., Abma,

647 W.R., Jetten, M.S.M., Loosdrecht, M.C.M. van, 2009. Emission of nitrous oxide and nitric oxide

648 from a full-scale single-stage nitritation-anammox reactor. Water Sci. Technol. 60, 3211–3217.

649 https://doi.org/10.2166/wst.2009.608

650 Kampschreur, M.J., van der Star, W.R.L., Wielders, H.A., Mulder, J.W., Jetten, M.S.M., van

651 Loosdrecht, M.C.M., 2008. Dynamics of nitric oxide and nitrous oxide emission during full-scale

652 reject water treatment. Water Res. 42, 812–826. https://doi.org/10.1016/j.watres.2007.08.022

653 Karatzoglou, A., Smola, A., Hornik, K., Zeileis, A., 2004. kernlab - An S4 Package for Kernel

654 Methods in R. J. Stat. Softw. 11, 1–20.

655 Lackner, S., Gilbert, E.M., Vlaeminck, S.E., Joss, A., Horn, H., van Loosdrecht, M.C., 2014.

656 Full-scale partial nitritation/anammox experiences–an application survey. Water Res. 55, 292–

657 303.

658 Law, Y., Lant, P., Yuan, Z., 2013. The Confounding Effect of Nitrite on N2O Production by an

659 Enriched Ammonia-Oxidizing Culture. Environ. Sci. Technol. 47, 7186–7194.

660 https://doi.org/10.1021/es4009689

661 Law, Y., Lant, P., Yuan, Z., 2011. The effect of pH on N 2 O production under aerobic conditions

662 in a partial nitrition system. Water Res. 45, 5934–5944.

663 Law, Y., Ye, L., Pan, Y., Yuan, Z., 2012. Nitrous oxide emissions from wastewater treatment

664 processes. Philos. Trans. R. Soc. B Biol. Sci. 367, 1265–1277.

665 https://doi.org/10.1098/rstb.2011.0317

666 Li, C., Wang, T., Zheng, N., Zhang, J., Ngo, H.H., Guo, W., Liang, S., 2013a. Influence of

667 organic shock loads on the production of N2O in denitrifying phosphorus removal process.

668 Bioresour. Technol., Challenges in Environmental Science and Engineering (CESE-2012) 141,

669 160–166. https://doi.org/10.1016/j.biortech.2013.03.117

670 Li, C., Zhang, J., Liang, S., Ngo, H.H., Guo, W., Zhang, Y., Zou, Y., 2013b. Nitrous oxide

671 generation in denitrifying phosphorus removal process: main causes and control measures.

672 Environ. Sci. Pollut. Res. 20, 5353–5360. https://doi.org/10.1007/s11356-013-1530-3

673 Liu, Y.-J., Gu, J., Liu, Y., 2018. Energy self-sufficient biological municipal wastewater

674 reclamation: Present status, challenges and solutions forward. Bioresour. Technol. 269, 513–519.

675 https://doi.org/10.1016/j.biortech.2018.08.104

676 Longo, S., d'Antoni, B.M., Bongards, M., Chaparro, A., Cronrath, A., Fatone, F., Lema, J.M.,

677 Mauricio-Iglesias, M., Soares, A., Hospido, A., 2016. Monitoring and diagnosis of energy

678 consumption in wastewater treatment plants. A state of the art and proposals for improvement.

679 Appl. Energy 179, 1251–1268. https://doi.org/10.1016/j.apenergy.2016.07.043

31

680   Luts, J., Ojeda, F., Van de Plas, R., De Moor, B., Van Huffel, S., Suykens, J.A.K., 2010. A

681   tutorial on support vector machine-based methods for classification problems in chemometrics.

682   Anal. Chim. Acta 665, 129–145. https://doi.org/10.1016/j.aca.2010.03.030

683   Massara, T.M., Malamis, S., Guisasola, A., Baeza, J.A., Noutsopoulos, C., Katsou, E., 2017. A

684   review on nitrous oxide (N 2 O) emissions during biological nutrient removal from municipal

685   wastewater and sludge reject water. Sci. Total Environ. 596, 106–123.

686   Newhart, K.B., Holloway, R.W., Hering, A.S., Cath, T.Y., 2019. Data-driven performance

687   analyses of wastewater treatment plants: A review. Water Res. 157, 498–513.

688   https://doi.org/10.1016/j.watres.2019.03.030

689   Pan, Y., Ni, B.-J., Bond, P.L., Ye, L., Yuan, Z., 2013. Electron competition among nitrogen

690   oxides reduction during methanol-utilizing denitrification in wastewater treatment. Water Res.

691   47, 3273–3281. https://doi.org/10.1016/j.watres.2013.02.054

692   Peng, L., Carvajal-Arroyo, J.M., Seuntjens, D., Prat, D., Colica, G., Pintucci, C., Vlaeminck, S.E.,

693   2017. Smart operation of nitritation/denitritation virtually abolishes nitrous oxide emission during

694   treatment of co-digested pig slurry centrate. Water Res. 127, 1–10.

695   https://doi.org/10.1016/j.watres.2017.09.049

696   Peng, L., Ni, B.-J., Ye, L., Yuan, Z., 2015. The combined effect of dissolved oxygen and nitrite

697   on N 2 O production by ammonia oxidizing bacteria in an enriched nitrifying sludge. Water Res.

698   73, 29–36.

699   Pijuan, M., Torà, J., Rodríguez-Caballero, A., César, E., Carrera, J., Pérez, J., 2014. Effect of

700   process parameters and operational mode on nitrous oxide emissions from a nitritation reactor

701   treating reject wastewater. Water Res. 49, 23–33. https://doi.org/10.1016/j.watres.2013.11.009

702 Raghavendra, N.S., Deka, P.C., 2014. Support vector machine applications in the field of

703 hydrology: A review. Appl. Soft Comput. 19, 372–386.

704 https://doi.org/10.1016/j.asoc.2014.02.002

705 Ren, Y., Ngo, H.H., Guo, W., Ni, B.-J., Liu, Y., 2019. Linking the nitrous oxide production and

706 mitigation with the microbial community in wastewater treatment: A review. Bioresour. Technol.

707 Rep. 7, 100191. https://doi.org/10.1016/j.biteb.2019.100191

708 Ribera-Guardia, A., Marques, R., Arangio, C., Carvalheira, M., Oehmen, A., Pijuan, M., 2016.

709 Distinctive denitrifying capabilities lead to differences in N2O production by denitrifying

710 polyphosphate accumulating organisms and denitrifying glycogen accumulating organisms.

711 Bioresour. Technol. 219, 106–113. https://doi.org/10.1016/j.biortech.2016.07.092

712 Rodriguez-Caballero, A., Aymerich, I., Marques, R., Poch, M., Pijuan, M., 2015. Minimizing

713 N2O emissions and carbon footprint on a full-scale activated sludge sequencing batch reactor.

714 Water Res. 71, 1–10. https://doi.org/10.1016/j.watres.2014.12.032

715 Rodriguez-Garcia, G., Frison, N., Vázquez-Padín, J.R., Hospido, A., Garrido, J.M., Fatone, F.,

716 Bolzonella, D., Moreira, M.T., Feijoo, G., 2014. Life cycle assessment of nutrient removal

717 technologies for the treatment of anaerobic digestion supernatant and its integration in a

718 wastewater treatment plant. Sci. Total Environ. 490, 871–879.

719 https://doi.org/10.1016/j.scitotenv.2014.05.077

720 Sarni, W., White, C., Webb, R., Cross, K., Glotzbach, R., 2019. Industry leaders chart the

721 transformation journey. International Water Association (IWA) and Xylem White Paper.

722 Schaubroeck, T., De Clippeleir, H., Weissenbacher, N., Dewulf, J., Boeckx, P., Vlaeminck, S.E.,

723 Wett, B., 2015. Environmental sustainability of an energy self-sufficient sewage treatment plant:

724   Improvements through DEMON and co-digestion. Water Res. 74, 166–179.

725   https://doi.org/10.1016/j.watres.2015.02.013

726   Schulthess, R. v., Kühni, M., Gujer, W., 1995. Release of nitric and nitrous oxides from

727   denitrifying activated sludge. Water Res. 29, 215–226. https://doi.org/10.1016/0043-

728   1354(94)E0108-I

729   Seshan, H., Goyal, M.K., Falk, M.W., Wuertz, S., 2014. Support vector regression model of

730   wastewater bioreactor performance using microbial community diversity indices: Effect of stress

731   and bioaugmentation. Water Res. 53, 282–296. https://doi.org/10.1016/j.watres.2014.01.015

732   Shi, S., Xu, G., 2018. Novel performance prediction model of a biofilm system treating domestic

733   wastewater based on stacked denoising auto-encoders deep learning network. Chem. Eng. J. 347,

734   280–290. https://doi.org/10.1016/j.cej.2018.04.087

735   Stenström, F., Tjus, K., Jansen, J. la C., 2014. Oxygen-induced dynamics of nitrous oxide in

736   water and off-gas during the treatment of digester supernatant. Water Sci. Technol. 69, 84–91.

737   https://doi.org/10.2166/wst.2013.558

738   Su, Q., Domingo-Félez, C., Zhang, Z., Blum, J.-M., Jensen, M.M., Smets, B.F., 2019. The effect

739   of pH on N2O production in intermittently-fed nitration reactors. Water Res. 156, 223–231.

740   https://doi.org/10.1016/j.watres.2019.03.015

741   Tallec, G., Garnier, J., Billen, G., Gousailles, M., 2006. Nitrous oxide emissions from secondary

742   activated sludge in nitrifying conditions of urban wastewater treatment plants: Effect of

743   oxygenation level. Water Res. 40, 2972–2980. https://doi.org/10.1016/j.watres.2006.05.037

744   van Loosdrecht, M.C.M., Salem, S., 2006. Biological treatment of sludge digester liquids. Water

745   Sci. Technol. J. Int. Assoc. Water Pollut. Res. 53, 11–20.

34

746 Vasilaki, V., Massara, T.M., Stanchev, P., Fatone, F., Katsou, E., 2019. A decade of nitrous oxide

747 (N2O) monitoring in full-scale wastewater treatment processes: A critical review. Water Res.

748 161, 392–412. https://doi.org/10.1016/j.watres.2019.04.022

749 Vasilaki, V., Volcke, E.I.P., Nandi, A.K., van Loosdrecht, M.C.M., Katsou, E., 2018. Relating

750 N2O emissions during biological nitrogen removal with operating conditions using multivariate

751 statistical techniques. Water Res. 140, 387–402. https://doi.org/10.1016/j.watres.2018.04.052

752 Wan, X., Baeten, J.E., Volcke, E.I.P., 2019. Effect of operating conditions on N2O emissions

753 from one-stage partial nitritation-anammox reactors. Biochem. Eng. J. 143, 24–33.

754 https://doi.org/10.1016/j.bej.2018.12.004

755 Wang, Y., Geng, J., Ren, Z., He, W., Xing, M., Wu, M., Chen, S., 2011. Effect of anaerobic

756 reaction time on denitrifying phosphorus removal and N2O production. Bioresour. Technol. 102,

757 5674–5684. https://doi.org/10.1016/j.biortech.2011.02.080

758 Wang, Z., Meng, Y., Fan, T., Du, Y., Tang, J., Fan, S., 2015. Phosphorus removal and N2O

759 production in anaerobic/anoxic denitrifying phosphorus removal process: Long-term impact of

760 influent phosphorus concentration. Bioresour. Technol. 179, 585–594.

761 https://doi.org/10.1016/j.biortech.2014.12.016

762 Zhou, X., Zhang, X., Zhang, Z., Liu, Y., 2018. Full nitration-denitration versus partial nitration-

763 denitration-anammox for treating high-strength ammonium-rich organic wastewater. Bioresour.

764 Technol. 261, 379–384. https://doi.org/10.1016/j.biortech.2018.04.049

765 Zhou, Y., Pijuan, M., Zeng, R.J., Yuan, Z., 2008. Free Nitrous Acid Inhibition on Nitrous Oxide

766 Reduction by a Denitrifying-Enhanced Biological Phosphorus Removal Sludge. Environ. Sci.

767 Technol. 42, 8260–8265. https://doi.org/10.1021/es800650j

768   Zhu, X., Chen, Y., 2011. Reduction of N2O and NO Generation in Anaerobic−Aerobic (Low

769   Dissolved Oxygen) Biological Wastewater Treatment Process by Using Sludge Alkaline

770   Fermentation Liquid. Environ. Sci. Technol. 45, 2137–2143. https://doi.org/10.1021/es102900h

Table 1: Influent and effluent concentrations of the SCENA system

	Parameter	unit	mean	Sd
SBR Influent	NH_4-N	mg/L	992.5	90
	PO_4-P	mg/L	30.8	6.9
	pH		8.2	0.2
	sCOD	mg/L	1111.7	562
	Flow-rate	m^3/d	30 (8.4 per cycle)	2.2
	Gas flow-rate	m^3/h	450 (170 - 520)	78
	Dimensions	mxmxm	8 x 3.5 x 2.5	
SBR Effluent	NH_4-N	mg/L	214.7	80.93
	NO_2-N	mg/L	3.23	9.7
	NO_3-N	mg/L	0.28	0.34
	PO_4-P	mg/L	6.78	2.22
	pH		8.04	0.3
SBR Reactor	MLSS	g/L	5.05	0.87
	HRT	d^{-1}	1.05	
	SRT	d^{-1}	15	
	pH		7.7	0.5
	T	°C	30.02	1.56
Fermentation Unit	NH_4-N	mg/L	715	72.6
	PO_4-P	mg/L	86	12
	pH		5.6	0.6
	T	°C	36	5.1
	sCOD	mg/L	13082	2228
	ferm_Hac	mg/L	3250	546
	ferm_HPr	mg/L	2281	588
	ferm_Hbut	mg/L	1347	196
	Flow-rate to SBR	m^3/cycle	7.45 (~2.41 per cycle)	3.0

Table 2: Features used in the classification algorithm to predict the accumulation of dissolved N_2O at the end of the anoxic and anaerobic phases

Anaerobic	Anoxic	Anaerobic regression
ORP phase initial	Last ORP value	ORP phase initial
ORP change	ORP change	ORP change
First local maximum ORP first derivative	Mean pH	
Local minimum of ORP first derivative after first local maximum ORP first derivative	Difference between first local maximum (after carbon dosage) and subsequent local minimum of the ORP first derivative	pH phase initial
Duration between first local maximum and subsequent local minimum of the ORP first derivative	Duration of carbon dosage	Time of ORP first derivative minimum/duration of phase
pH phase initial	Duration between first local maximum (after carbon dosage) and subsequent local minimum of the ORP first derivative	Difference between first local maximum and subsequent local minimum of the ORP first derivative
Time local minimum ORP first derivative/Phase duration	Last ORP first derivate	

Table 4: Features selected in the SVR model for the aerobic phase

Aerobic Features
Average conductivity rate
ORP end of aeration
ORP increase during aeration
Conductivity at the beginning of aeration
Average DO
pH at the beginning of aeration
Conductivity increase (based on the conductivity at the end of the aerobic phase of the previous cycle)
pH change during aeration
Initial aerobic N_2O concentration (based on ANSVR predictions)

Table 3: SVM classification results anoxic and anaerobic phases

| Phase	Dataset	Misclassified	Sensitivity	Specificity	Accuracy (%)	Kappa	Class
Anoxic phase cycle N	Train	anoxA: 1 anoxB: 0	1	0.99	99	0.97	anoxA: Final dissolved N_2O concentration end of anoxic < 0.6 mg/L
	Test	anoxA: 1 anoxB: 0	1	0.98	98	0.92	
							anoxB: Final dissolved N_2O concentration end of anoxic > 0.6 mg/L
Anaerobic phase cycle N+1	Train	anaerA:2 anaerB: 1	0.98	0.97	97	0.94	anaerA: N_2O end of anaerobic > 2.6 mg/L
	Test	anaerA: 1 anaerB: 0	1	0.97	98	0.95	anaerB: N_2O end of anaerobic < 2.6 mg/L
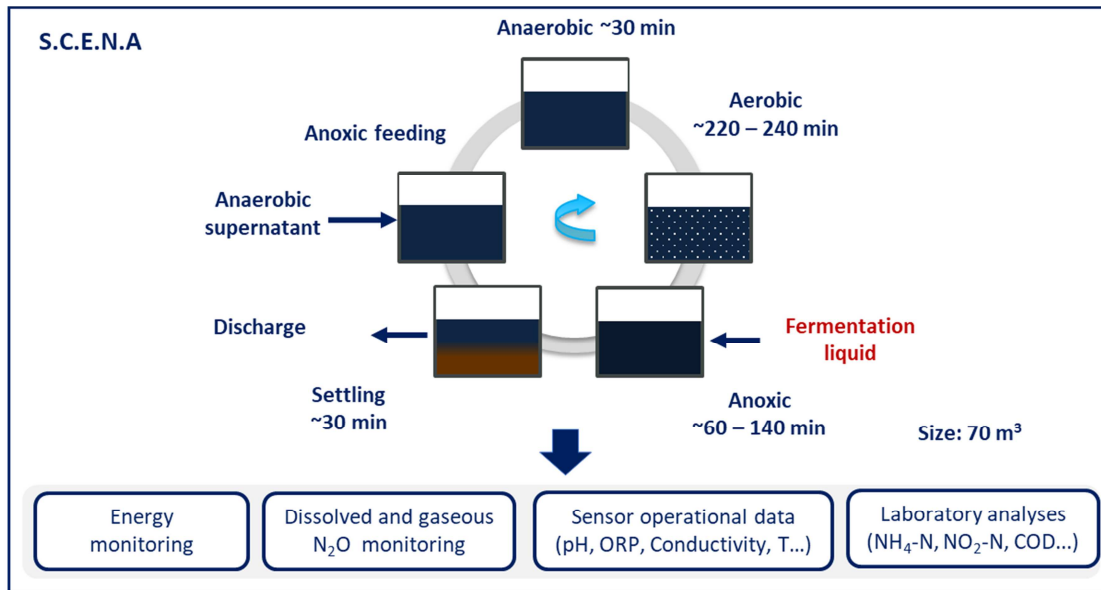
Figure 1: Schematic representation of a complete cycle in the S.C.E.N.A process and datasets

used in the analysis
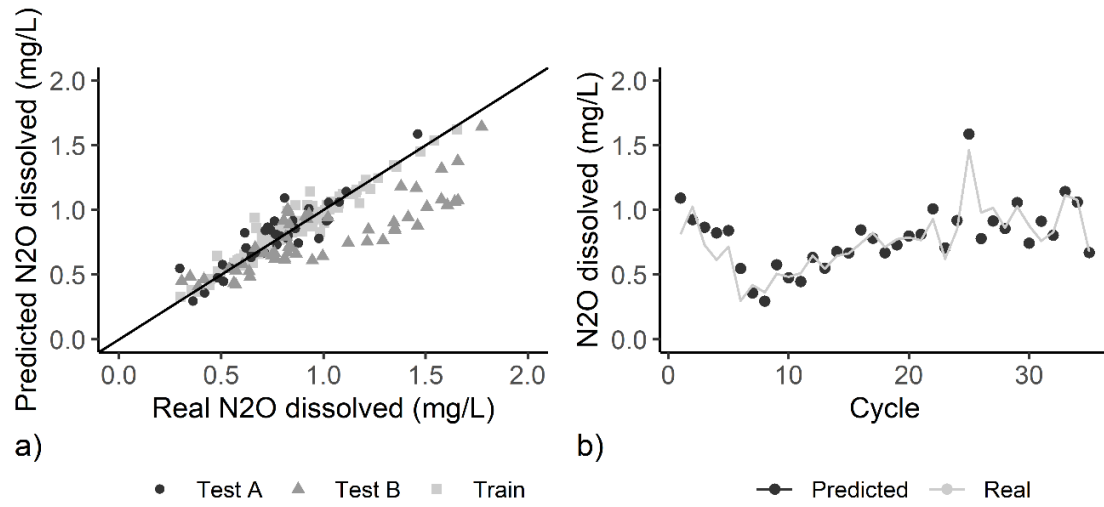
Figure 10: (a) Predicted vs measured dissolved N2O concentration (AERSVR) in the aerobic phase for the train dataset, the test dataset A and the test dataset B and (b) comparison of predicted and measured dissolved N2O concentration for the test dataset B
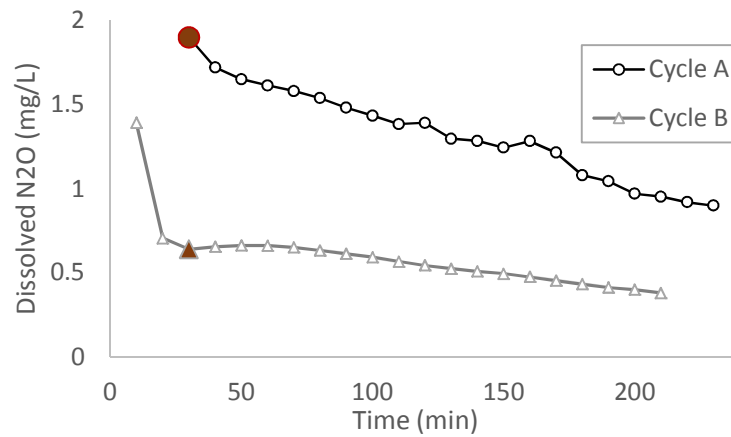
Figure 11: An example of dissolved N2O profiles for cycles belonging to anaerB cycles (test

dataset B). The red points represent the first point considered for the calculation of the average

aerobic N_2O accumulation (as described in section 2.2.1). Data points in the beginning of aeration

exceeding sensor calibration limits are not shown.

Phase 1: Preprocessing– Outliers detection

- Dissolved and gaseous N_2O monitoring
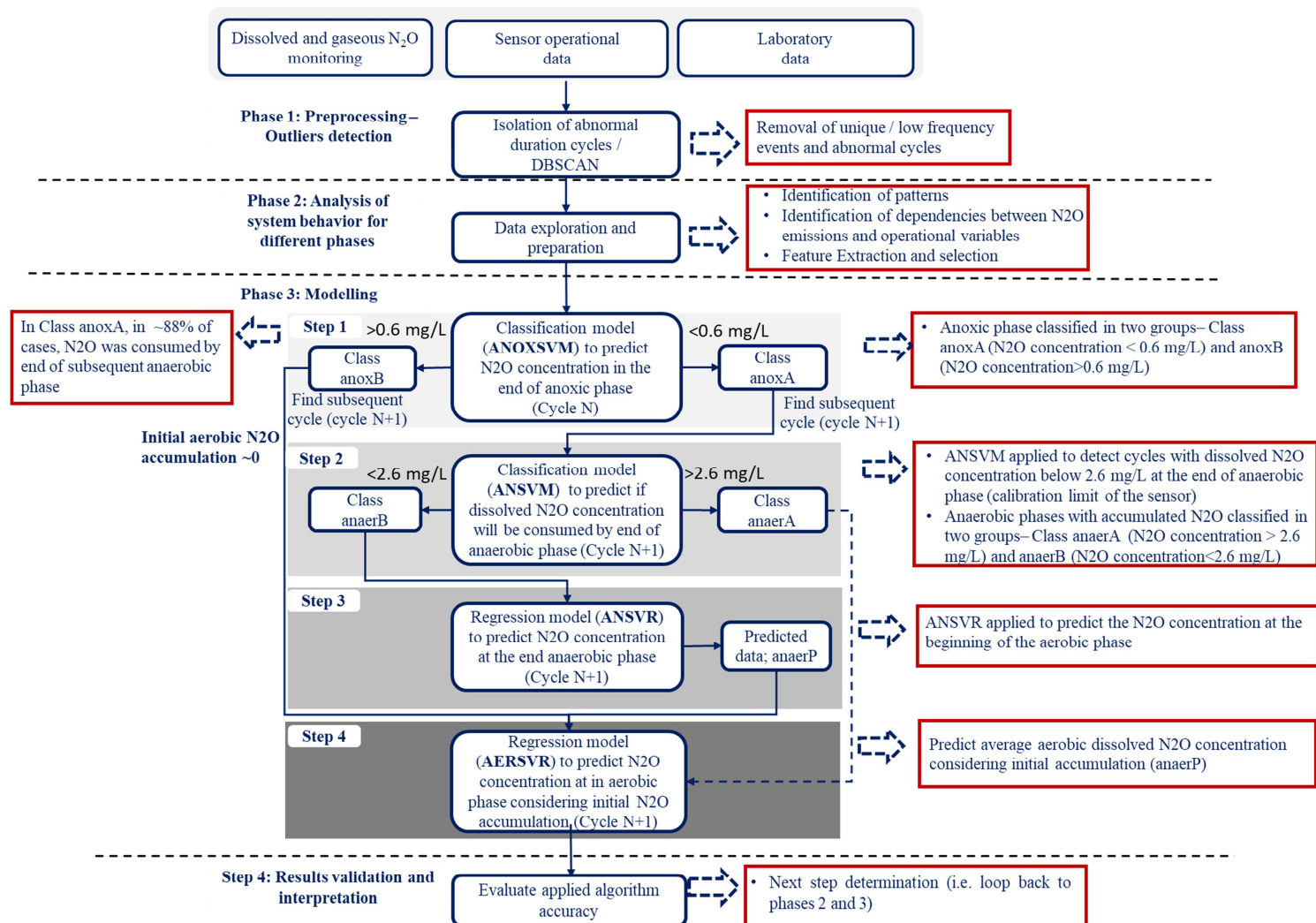- Sensor operational data
- Laboratory data

Isolation of abnormal duration cycles / DBSCAN → Removal of unique / low frequency events and abnormal cycles

Phase 2: Analysis of system behavior for different phases

Data exploration and preparation →
- Identification of patterns
- Identification of dependencies between N2O emissions and operational variables
- Feature Extraction and selection

Phase 3: Modelling

In Class anoxA, in ~88% of cases, N2O was consumed by end of subsequent anaerobic phase

Step 1 >0.6 mg/L — Classification model (**ANOXSVM**) to predict N2O concentration in the end of anoxic phase (Cycle N) — <0.6 mg/L

Class anoxB ← Find subsequent cycle (cycle N+1)

Class anoxA → Find subsequent cycle (cycle N+1)

- Anoxic phase classified in two groups– Class anoxA (N2O concentration < 0.6 mg/L) and anoxB (N2O concentration>0.6 mg/L)

Initial aerobic N2O accumulation ~0

Step 2 <2.6 mg/L — Classification model (**ANSVM**) to predict if dissolved N2O concentration will be consumed by end of anaerobic phase (Cycle N+1) — >2.6 mg/L

Class anaerB

Class anaerA

- ANSVM applied to detect cycles with dissolved N2O concentration below 2.6 mg/L at the end of anaerobic phase (calibration limit of the sensor)
- Anaerobic phases with accumulated N2O classified in two groups– Class anaerA (N2O concentration > 2.6 mg/L) and anaerB (N2O concentration<2.6 mg/L)

Step 3 Regression model (**ANSVR**) to predict N2O concentration at the end anaerobic phase (Cycle N+1) → Predicted data; anaerP

ANSVR applied to predict the N2O concentration at the beginning of the aerobic phase

Step 4 Regression model (**AERSVR**) to predict N2O concentration at in aerobic phase considering initial N2O accumulation (Cycle N+1) → Predict average aerobic dissolved N2O concentration considering initial accumulation (anaerP)

Step 4: Results validation and interpretation

Evaluate applied algorithm accuracy →
- Next step determination (i.e. loop back to phases 2 and 3)
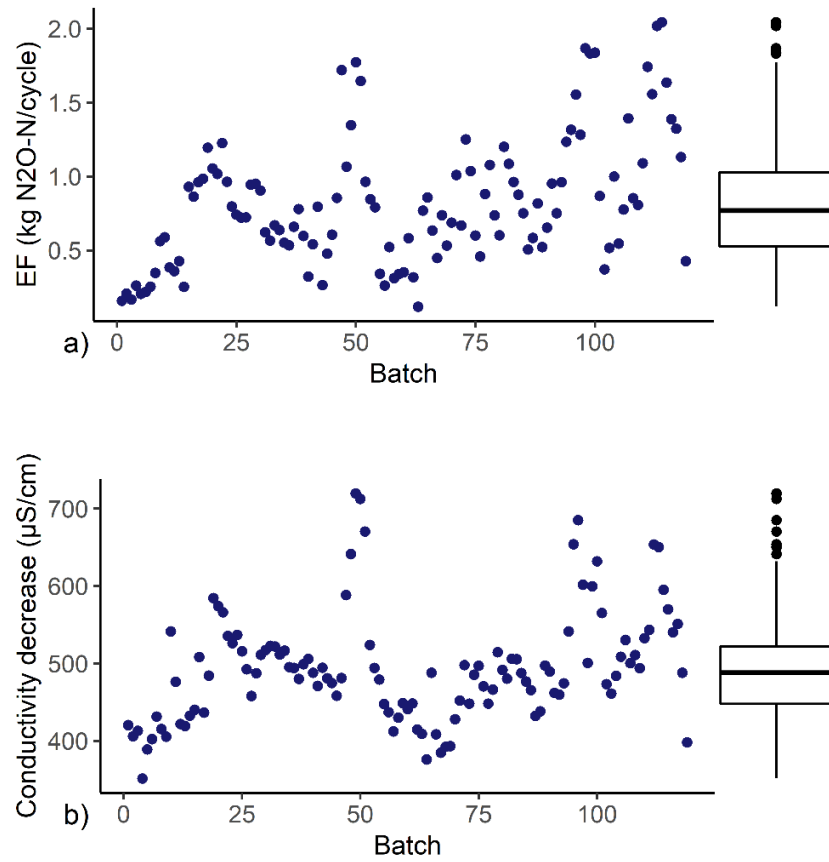
Figure 2: Methodological Framework followed in the study

Figure 3: (a) N$_2$O emissions and (b) aerobic phase conductivity decrease, during monitoring

campaign (gas analyser, March-April)

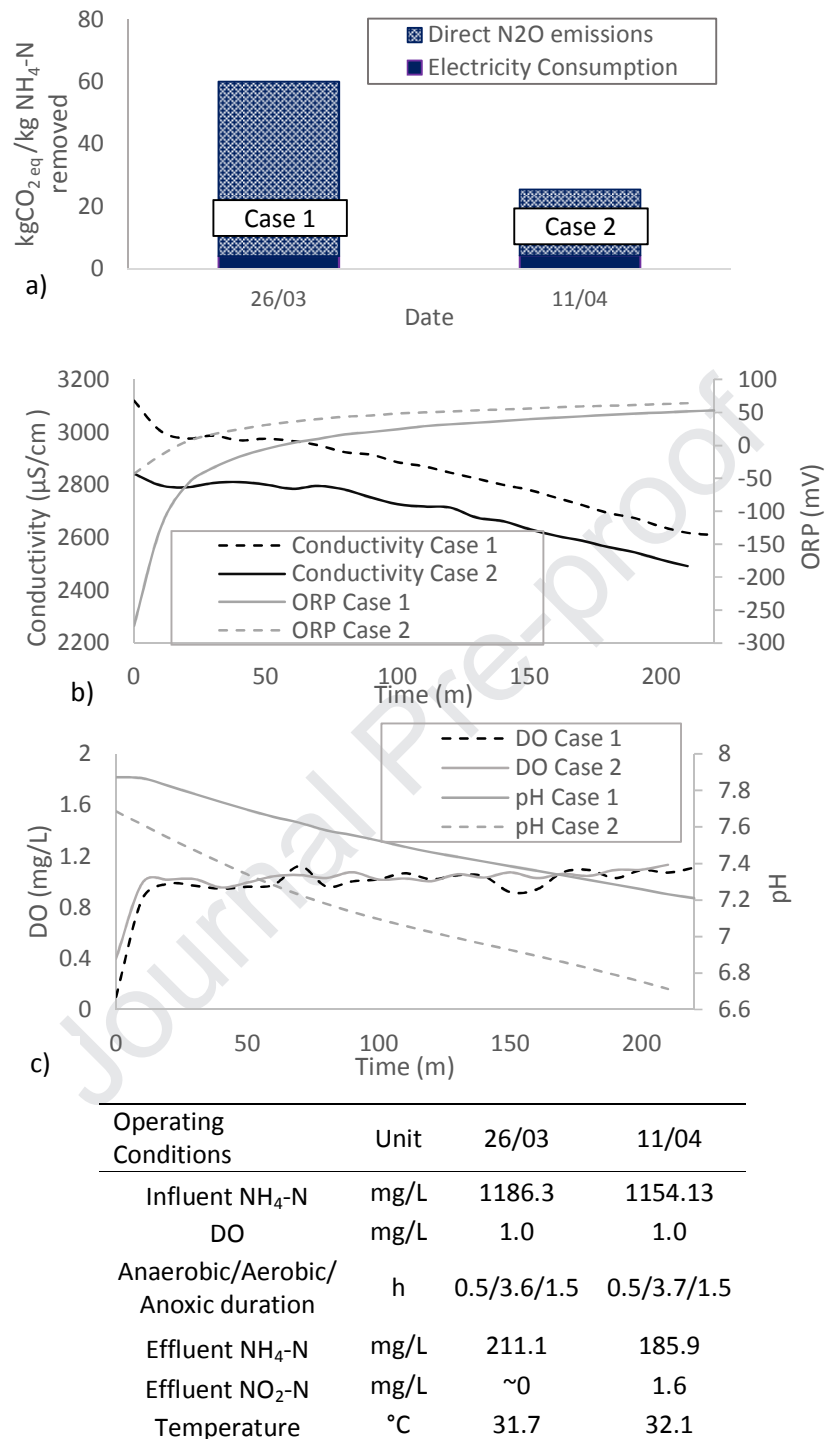Figure 4: (a) Example of the effect of N₂O emissions in the operational carbon footprint for two cases, (b) aerobic profiles of conductivity, ORP and (c) DO for the two cases shown in (a)
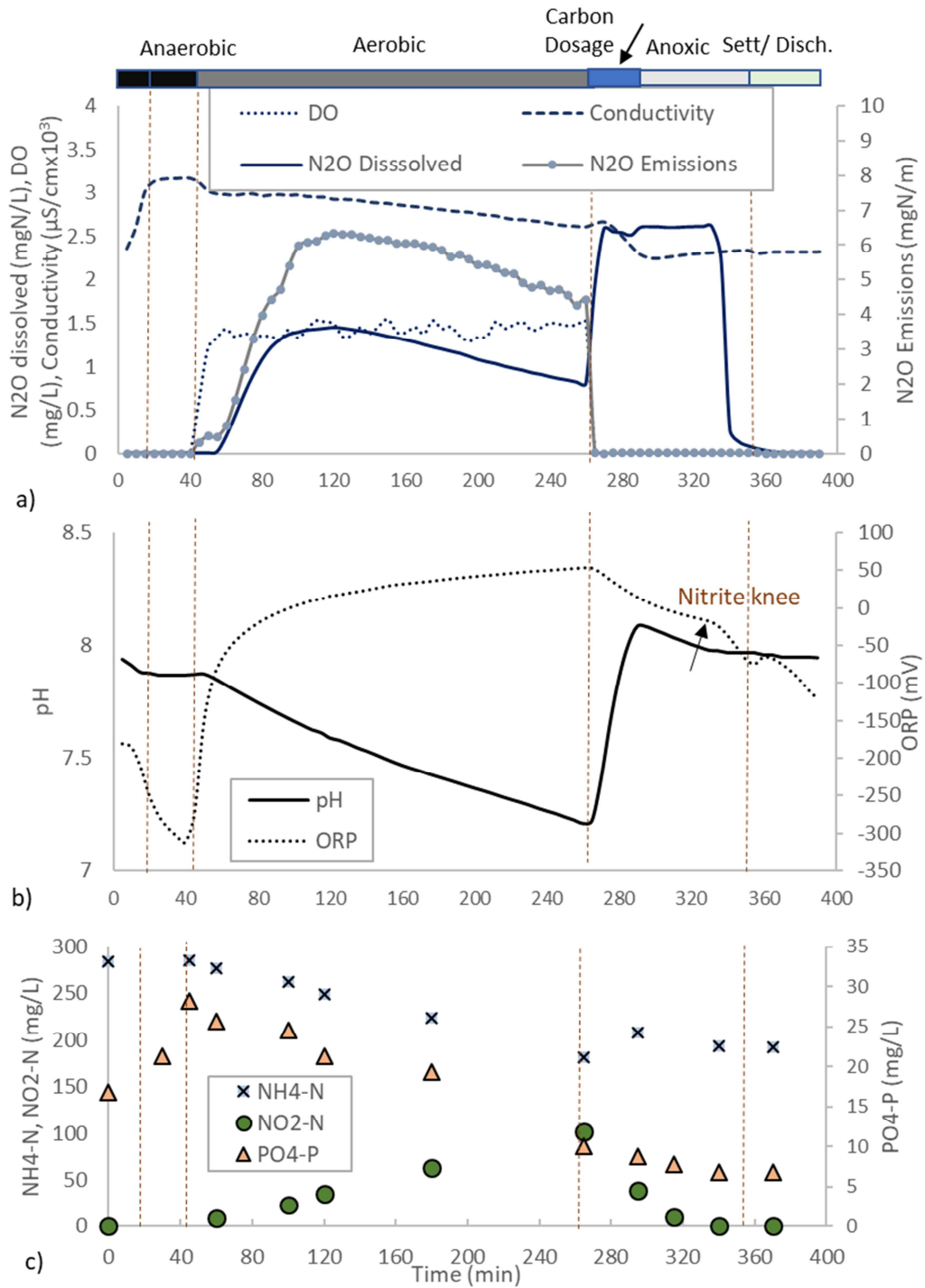
Operating Conditions	Unit	26/03	11/04
Influent NH$_4$-N	mg/L	1186.3	1154.13
DO	mg/L	1.0	1.0
Anaerobic/Aerobic/ Anoxic duration	h	0.5/3.6/1.5	0.5/3.7/1.5
Effluent NH$_4$-N	mg/L	211.1	185.9
Effluent NO$_2$-N	mg/L	~0	1.6
Temperature	°C	31.7	32.1

Figure 4: (a) Example of the effect of N$_2$O emissions in the operational carbon footprint for two cases, (b) aerobic profiles of conductivity, ORP and (c) DO for the two cases shown in (a)

Figure 5: Representative cycle profile for the (a) dissolved N_2O concentration, N_2O emissions, conductivity, DO, (b) ORP and pH, and (c) NH_4-N, NO_2-N and PO_4-P concentrations
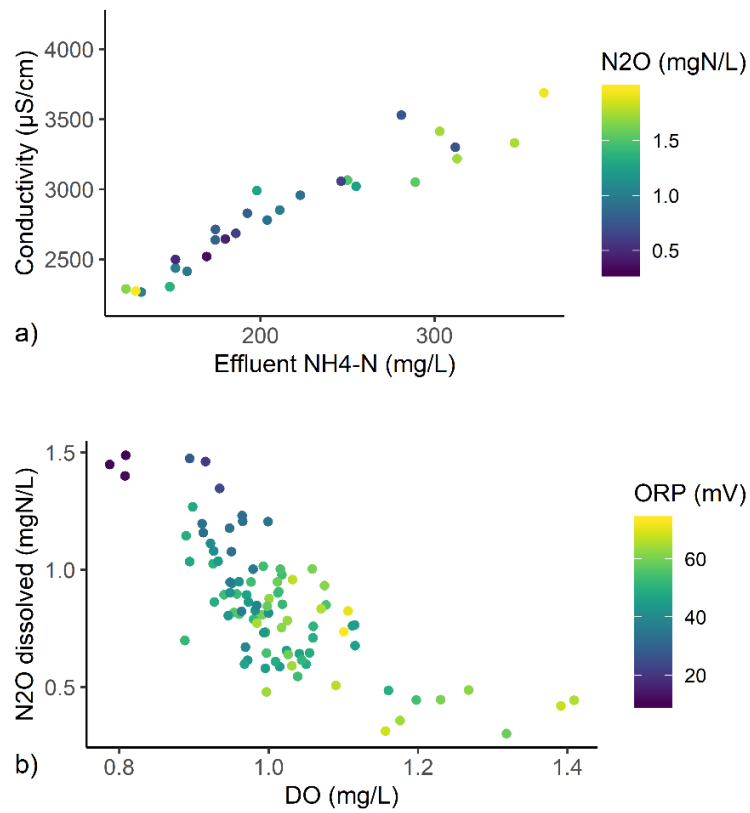
Figure 6: (a) Daily average conductivity at the end of the aerobic phase versis effluent NH$_4$-N concentration (coloured points: average dissolved N$_2$O accumulated in the aerobic phase), (b) Aerobic average accumulated dissolved N$_2$O in respect to DO concentration; only cycles without initial N$_2$O accumulation from the previous anoxic cycle are shown (coloured points: ORP at the end of the aerobic phase)
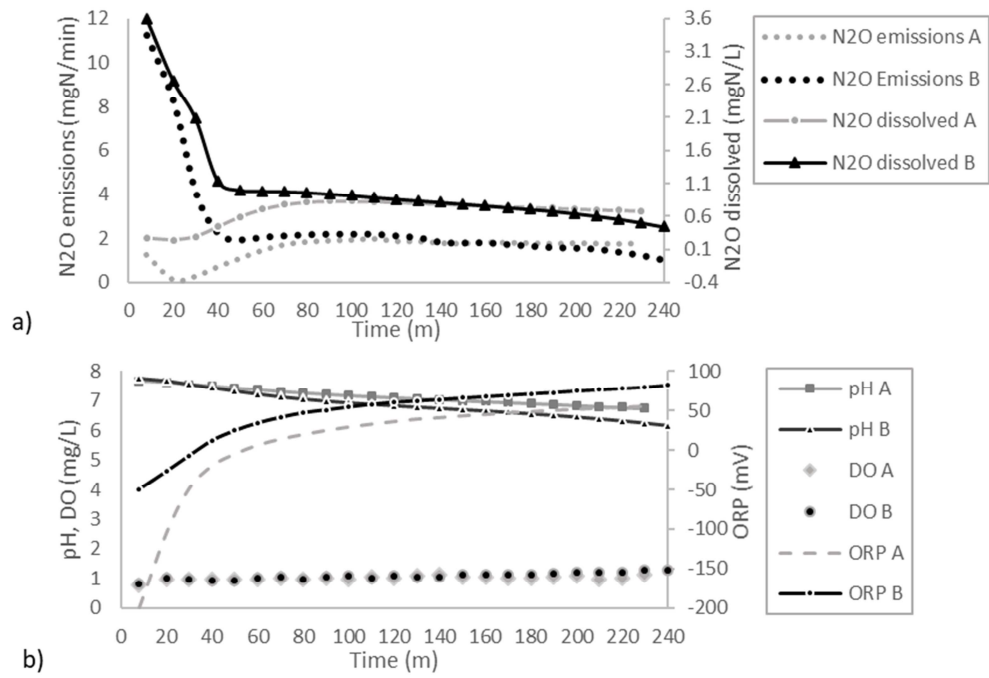
Figure 7: (a) Representative profiles of dissolved N_2O concentration based on different initial

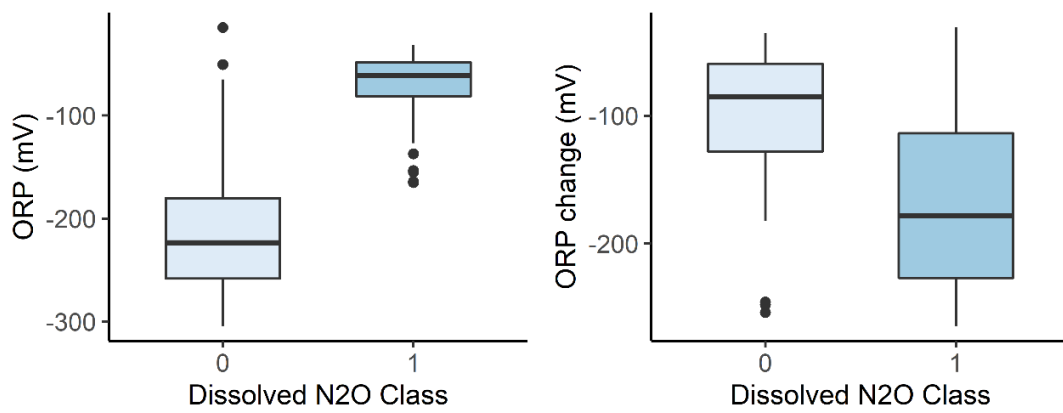concentrations of N_2O in the beginning of the aerobic phase and (b) ORP and DO profiles

Figure 8: Box-plots of the (a) initial anaerobic ORP and (b) the ORP change during the anaerobic phase for cycles with and without N_2O consumption (Class 0: no significant N_2O consumption or anaerobic N_2O concentration > 2.6 mg/L; Class 2: significant N_2O consumption)
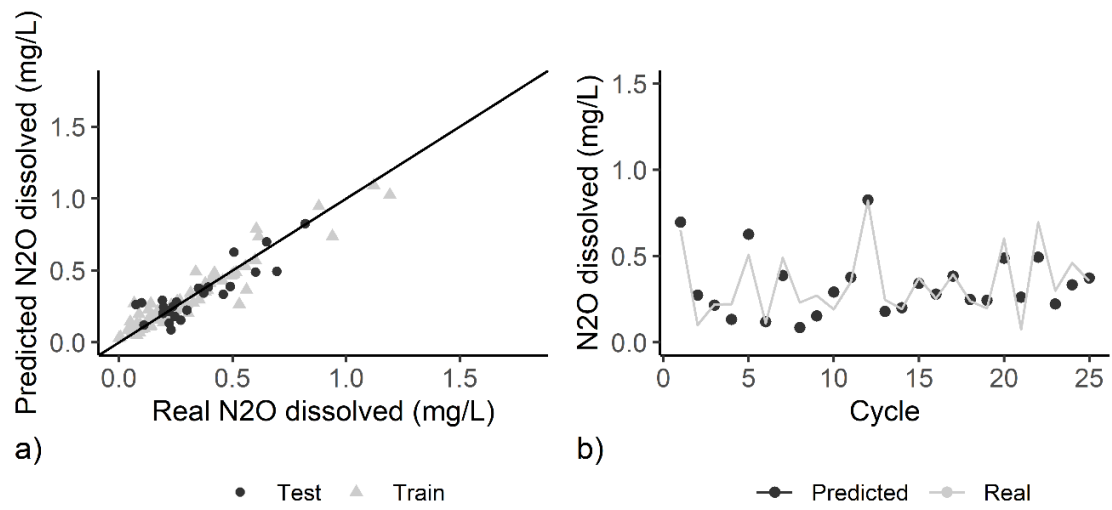
Figure 9: (a) Predicted vs measured dissolved N_2O concentration in the end of the anaerobic phase (ANSVR) for the test and train datasets and (b) comparison of predicted and measured dissolved N_2O concentration for the test dataset

Highlights

- S.C.E.N.A N_2O emissions contribute up to 97.3% to the operational carbon footprint

- Stripping of accumulated N_2O from the previous anoxic cycle increases emissions

- Aerobic dissolved N_2O concentration is correlated with DO and conductivity

- Conductivity can be used to control SBR NH_4^+ concentration and N_2O

- N_2O can be estimated as a latent parameter from other low-cost sensors

Declaration of interests

☒ The authors declare that they have no known competing financial interests or personal relationships that could have appeared to influence the work reported in this paper.

☐The authors declare the following financial interests/personal relationships which may be considered as potential competing interests: